# Tuning Electron Density of Active Site for Enhanced Molecular Recognition and Catalysis

Foroogh Bahrami and Yan Zhao*

Department of Chemistry, Iowa State University, Ames, Iowa 50011-3111, U.S.A.

**ABSTRACT:** Enzymes have an extraordinary ability to utilize aromatic interactions for molecular recognition and catalysis. We here report molecularly imprinted nanoparticle receptors. The aromatic "wall" material in the imprinted binding site is used to enhance the molecular recognition of aromatic guests that have similar charge, shape, and size but differ in π electron density. Additionally, aromatic interactions are employed to activate an electron-rich aryl leaving group on a glycoside, mimicking the nucleoside hydrolase of the parasite Trypanosoma vivax.

**KEYWORDS:** *aromatic interactions, enzyme mimetics, molecular imprinting, artificial enzyme, active site*

Abundant in both synthetic and natural materials, aromatic groups may interact with other aromatic groups through π–π interactions in different geometries.[1] They can also interact with cations[2] or anions,[3] depending on their electron densities. These interactions have been used extensively in supramolecular hosts and synthetic catalysts over the years.[1-6]

Enzymes have extraordinary abilities to exploit aromatic interactions for their catalysis. Glycosidases, for example, frequently have an aromatic group in their active sites to help stabilize the glycoside cationic transition states during the hydrolysis.[7,8] Flavodoxins utilize an unfavorable π–π stacking aromatic interaction to lower the reduction potential of its catalytic cofactor.[9] In this work, we report polymeric nanoparticle receptors and artificial enzymes that utilize aromatic interactions for enhanced molecular recognition and catalysis. An artificial glycosidase is shown to override the intrinsic reactivity of aryl glycosides through favorable π–π interactions, so that a less reactive substrate becomes more reactive in the catalysis.

Our nanoparticles receptors and catalysts were prepared through molecular imprinting, a method to create template-complementary pockets or imprinted sites in a cross-linked polymer network.[10-19] To obtain protein-mimicking water-soluble imprinted nanoparticles, we performed molecular imprinting inside the surfactant micelles of **1a**–**c**. These cationic micelles easily incorporate anionic aromatic template molecules such as **T1** or **T2**,[20] along with divinyl benzene (DVB, a radical cross-linker) and 2,2-dimethoxy-2-phenylacetophenone (DMPA, a photoinitiator). They are first cross-linked on the surface using diazide **2** and then functionalized with monoazide **3**, both via the highly efficient click reaction (Scheme 1a). UV irradiation then initiates free radical polymerization of the micellar core around the template molecule, among the methacrylates of the surfactants and DVB. The anionic sulfonate group on the template acts as a hydrophilic anchor in this process, due to its preference for the surface of the micelle and ion-pairing interactions with the ammonium headgroup of the surfactant. Through this strategy, the imprinted site is formed near the surface of the resulting molecularly imprinted nanoparticle (MINP), to facilitate template removal during purification and mass transfer in the subsequent binding or catalysis.

Table 1 shows the binding constants determined by isothermal titration calorimetry (ITC). MINP$_{1a}$(**T1**) designates the imprinted nanoparticle prepared using **T1** as the template and **1a** as the cross-linkable surfactant. **T1** and **T2** are the model aromatic compounds in this study, to probe the molecular recognition of the MINPs. These two compounds have the same substitution pattern except one is electron-deficient with the nitro group and the other electron-rich with the methoxy. They are chosen specifically to understand the electron properties of the imprinted binding sites.

Surfactant **1a**, a previously reported surfactant,[21-23] does not contain any aromatic group, although the click cross-linking and surface-functionalization will install triazole groups near the ammonium headgroup in the final MINPs. As shown by entries 1 and 2 of Table 1, MINP$_{1a}$(**T1**) binds its template (**T1**) strongly, it has difficulty distinguishing **T1** and **T2**. The relative binding constant ($K_{rel}$), i.e., the binding constant of a guest relative to that of the template, is 0.92 (entry 2). The lack of selectivity in this case is not a surprise, given that the main driving force for the binding (in water) is the hydrophobic interactions derived from the aromatic group of the guest entering a complementary hydrophobic pocket, supplemented by the electrostatic interactions between the anionic sulfonate and the cationic ammonium headgroups of the cross-linked surfactants. These driving forces for both **T1** and **T2** are apparently very similar.

When **1b** is used as the cross-linkable surfactant, the resulting MINP$_{1b}$(**T1**) shows a reversed selectivity, with its binding for **T2** 1.8 times stronger than that for template **T1** (entry 4). This result is actually what we hoped to see, because it indicates that the electron-deficient aromatic ring near the ammonium headgroup of **1b** is able to influence the electron density of the imprinted binding site, making it prefer the electron-rich guest (**T2**) over its own template (**T1**). Meanwhile, MINP$_{1b}$(**T2**), the nanoparticle receptor made with the electron-rich **T2** as the template, has an excellent selectivity, because the similarly sized electron-deficient **T1** is only bound with a $K_{rel}$ of 0.11 (entry 6). Thus, our MINP receptor always prefers the electron-rich guest, regardless of the template used, suggesting that the imprinted site is formed near the electron-deficient aromatic ring of the surfactants, consistent with our hydrophilic anchoring strategy mentioned above. (As will be shown in the later sections, such a feature is critical to our biomimetic activation of the aryl leaving group.)

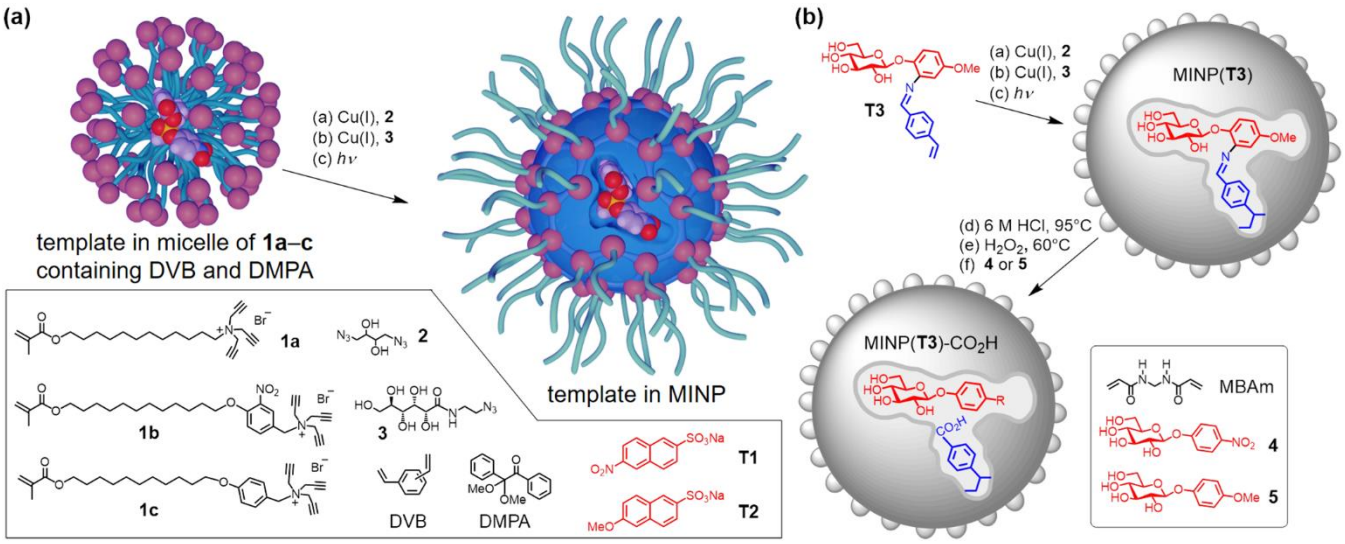


**Scheme 1.** Preparation of molecularly imprinted nanoparticles (MINPs) (a) for binding aromatic guests **T1** and **T2** and (b) for catalyzing the hydrolysis of aryl β-D-glucopyranosides **4** or **5**. The surface ligand (**3**) is omitted for clarity in Scheme 1b.

**Table 1.** ITC binding data for guest **T1** and **T2** by different MINPs determined by ITC.[a]

| entry | host | guest | $K_a$ ($\times 10^6$ $M^{-1}$) | $K_{rel}$[b] |
|---|---|---|---|---|
| 1 | $MINP_{1a}$(**T1**) | T1 | 1.18 ± 0.22[c] | 1 |
| 2 | $MINP_{1a}$(**T1**) | T2 | 1.08 ± 0.06 | 0.92 |
| 3 | $MINP_{1b}$(**T1**) | T1 | 2.28 ± 0.19 | 1 |
| 4 | $MINP_{1b}$(**T1**) | T2 | 4.06 ± 0.22 | 1.8 |
| 5 | $MINP_{1b}$(**T2**) | T2 | 10.0 ± 0.64 | 1 |
| 6 | $MINP_{1b}$(**T2**) | T1 | 1.06 ± 0.09 | 0.11 |
| 7 | $MINP_{1c}$(**T1**) | T1 | 2.93 ± 0.24 | 1 |
| 8 | $MINP_{1c}$(**T1**) | T2 | 2.18 ± 0.23 | 0.74 |
| 9 | $MINP_{1c}$(**T2**) | T2 | 2.65 ± 0.20 | 1 |
| 10 | $MINP_{1c}$(**T2**) | T1 | 2.48 ± 0.15 | 0.94 |
| 11 | $MINP_{1b,c}$(**T1**) | T1 | 1.88 ± 0.10 | 1 |
| 12 | $MINP_{1b,c}$(**T1**) | T2 | 1.08 ± 0.12 | 0.57 |
| 13 | $MINP_{1b,c}$(**T2**) | T2 | 3.57 ± 0.30 | 1 |
| 14 | $MINP_{1b,c}$(**T2**) | T1 | 1.55 ± 0.09 | 0.43 |

[a] The titrations were performed in duplicates in 25 mM HEPES buffer (pH 7.0) at 25 °C (see Table S2 and Figures S5–S17 for details), and the errors between the runs were <20%. [b] $K_{rel}$ is the binding constant of a guest relative to that of the templating for a particular MINP.

The nitro group on the aromatic ring in the cross-linkable surfactant is essential to the observed selectivity for electron-rich aromatics. Without it, neither $MINP_{1c}$(**T1**) nor $MINP_{1c}$(**T2**) shows good selectivity, with the $K_{rel}$ value being 0.74 and 0.94, respectively (entries 8 and 10). Hence, without the electron-withdrawing group on the aromatic ring, the MINP has difficulty distinguishing the two aromatic guests. The electron density of the imprinted binding site can be tuned additionally using a mixture of **1b** and **1c** as the surfactant. With a 1:1 mixture of the two, $MINP_{1b,c}$(**T1**) and $MINP_{1b,c}$(**T2**) prefer their own templates over the competing guests, albeit with still a modest selectivity (entries 12 and 14, $K_{rel}$ = 0.57 and 0.43, respectively).

Having confirmed the ability to tune the electron density of the imprinted site through the cross-linkable surfactant, we set out to create a synthetic glycosidase[24-27] to mimic the nucleosidehydrolase of the parasite Trypanosoma vivax.[28] This particular enzyme employs aromatic interactions from two tryptophans to activate the leaving group (a purine base) on its substrate.

Our synthetic glycosidase was prepared according to Scheme 1b, using **T3** as the template. To help bind the amphiphilic sugar derivative, we included a water-soluble cross-linker, *N*,*N*′-methylenebisacrylamide (MBAm), in the micellar solution. Because the hydrophobic DMPA photoinitiator prefers the interior of the micelle, the propagating radical is confined within the micelle and can only polymerize MBAm molecules when they diffuse to the surface of the micelle. Some of these polymerized MBAm molecules are fixed in the guest-binding configurations near the surfactant/water interface during the imprinting process, and can help bind the template with hydrogen bonds. Previously, inclusion of MBAm in the formulation has been shown to strengthen the MINP binding for 4-nitrophenyl-α-D-glucopyranoside by 180-fold.[29]

As shown in Scheme 1b, the MINP(**T3**) obtained is treated with 6 M HCl at 95 °C to hydrolyze the imine bond. With the vinyl group polymerized into the micellar core by free radical polymerization, the imine hydrolysis yields an aldehyde group in the imprinted site. The resulting MINP(**T3**)–CHO is then oxidized using an excess (50 equiv., Table S1) of hydrogen peroxide to afford MINP(**T3**)–$CO_2H$, a "synthetic enzyme" designed to bind aryl glucoside **4** or **5** and cleave the glycosidic bond by the nearby carboxylic acid. Many enzymes including glycosidases[30] and aspartic proteases[31] utilize carboxylic acids in their active sites for catalysis. In this study, our primary goal was to employ aromatic interactions to assist the activation of the aryl leaving group by the nearby carboxylic acid through a general acid catalysis.[30]

Figure 1 shows that $MINP_{1b}$(**T3**)–$CO_2H$ indeed is able to hydrolyze 4-nitrophenyl β-D-glucopyranoside (**4**) much better than the two controls in pH 6 buffer. The reaction is monitored by UV-vis

**Table 2.** Michaelis–Menten parameters the hydrolysis of aryl β-D-glucopyranosides by MINP and other catalysts.[a]

| entry | catalyst | substrate | pH | *temp.* (°C) | $k_{cat}$ ($min^{-1}$) | $K_m$ (μM) | $k_{cat}/K_m$ ($M^{-1}s^{-1}$) | note |
|---|---|---|---|---|---|---|---|---|
| 1 | $MINP_{1b}$(**T3**)-$CO_2H$ | **4** | 6.0 | 40 | 0.158 ± 0.009 | 234 ± 23 | 11.1 | this work |
| 2 | $MINP_{1b}$(**T3**)-$CO_2H$ | **5** | 6.0 | 40 | 0.155 ± 0.005 | 69 ± 6 | 37.7 | this work |
| 3 | $MINP_{1a}$(**T3**)-$CO_2H$ | **4** | 6.0 | 40 | 0.124 ± 0.013 | 204 ± 37 | 10.3 | this work |
| 4 | $MINP_{1a}$(**T3**)-$CO_2H$ | **5** | 6.0 | 40 | 0.011 ± 0.001 | 184 ± 15 | 1.1 | this work |
| 5 | cyclodextrin cyanohydrin | **4** | 7.4 | 59 | 0.0018 | 5400 | $5.6 \times 10^{-3}$ | ref 24 |
| 6 | copper-containing microgel | **4** | 10.5 | 30 | 0.129 | 6000 | 0.37 | ref 25 |
| 7 | β-glucosidase from *Streptomyces venezuelae* | **4** | 8.0 | 25 | 800 | 9100 | 1500 | ref 36 |
| 8 | β-glucosidase from *Serratia sp. TN49* | **4** | 7.5 | 35 | 1360 | 7790 | 2910 | ref 37 |
| 9 | β-glucosidase from *Bifdobacterium adolescentis* | **4** | 6.5 | 30 | 5280 | 320 | $2.75 \times 10^5$ | ref 38 |

[a] Hydrolysis by MINP catalysts was performed in a 10 mM MES buffer (pH 6.0) at 40 °C. [MINP] = 8.0 μM. The full data are reported in the supporting information (Figures S19–S27).

spectroscopy at 320 nm for the release of the *p*-nitrophenol product. $MINP_{1b}$(**T3**)–CHO, the intermediate MINP obtained after the imine hydrolysis in Scheme 1b, contains an aldehyde group in the imprinted site and has a slightly higher activity than the nonimprinted nanoparticles (NINPs) prepared without any template. Yet both control nanoparticles are far less active than $MINP_{1b}$(**T3**)–$CO_2H$ that has the acid group in the active site.

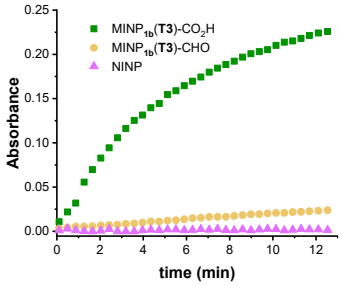


**Figure 1.** Hydrolysis of 4-nitrophenyl β-D-glucopyranoside (**4**) by different nanoparticles in a 10 mM MES buffer (pH 6.0) at 40 °C. [**4**] = 50 μM. [catalyst] = 5.0 μM.

The rate constant for the catalytic hydrolysis of **4** by $MINP_{1b}$(**T3**)–$CO_2H$ is nearly constant over pH 5.5–6.0 but falls off rapidly over pH 6.0–6.5 (Figure S19a). Carboxylic acids typically have a p$K_a$ around 4–5 in solution. The p$K_a$ for $MINP_{1b}$(**T3**)–$CO_2H$ is clearly higher (>6.0) based on the pH profile. The result is reasonable because the microenvironment around an acid/base strongly impacts its acidity/basicity, whether inside an enzyme[32] or a synthetic host.[33-35] Since an ionic carboxylate is better solvated by water than a neutral carboxylic acid, the p$K_a$ of a carboxylic acid shifts higher when it resides in a hydrophobic microenvironment and is observed in our catalyst.

$MINP_{1b}$(**T3**)–$CO_2H$ displays saturation behavior in its catalysis, similar to enzymes (Figures S19–27). Its Michaelis constant ($K_m$) for the catalytic hydrolysis of **4** is measured to be 234 ± 23 μM and the catalytic turnover ($k_{cat}$) 0.158 ± 0.009$min^{-1}$, affording a catalytic efficiency ($k_{cat}/K_m$) of 11.1 $M^{-1}s^{-1}$ (Table 2, entry 1).

4-Methoxyphenyl β-D-glucopyranoside (**5**) has a poorer leaving group than **4** and is expected to be less reactive. However, $MINP_{1b}$(**T3**)–$CO_2H$ catalyzes its hydrolysis with $k_{cat}/K_m$ = 37.7 $M^{-1}s^{-1}$, more than 3 times higher than the catalytic efficiency for **4** (Table 2, entries 1 and 2).

Once the aromatic group is eliminated from the surfactant, $MINP_{1a}$(**T3**)–$CO_2H$ displays the normal reactivity trend for the two substrates. Entries 3 and 4 of Table 2 indicate that the catalytic efficiency of **4** is 9.4 times higher than that of **5** (entries 3 and 4) in the absence of the aromatic activation. Since the substrate binding ($K_m$) for the two substrates is very similar with $MINP_{1a}$(**T3**)–$CO_2H$, the main difference in $k_{cat}/K_m$ is caused by the higher catalytic turnover ($k_{cat}$), which is 11 times higher for **4** than for **5**.

In the literature, different substrates are often used to evaluate the catalytic efficiency of artificial glycosidases. Among the artificial enzymes that employ 4-nitrophenyl β-D-glucopyranoside (**4**), our catalysts compare favorably although different reaction conditions make direct comparison impossible. It should be noted that natural β-glucosidases are far more active than any of the synthetic catalysts reported, with catalytic efficiencies in the range of $k_{cat}/K_m$ = 1500 to $2.75 \times 10^5$ $M^{-1}s^{-1}$ (Table 2, entries 7–9).[36-38]

Carbohydrates are the most abundant organic molecules on the earth. Although much improvement is needed for the synthetic glycosidases, it is encouraging that a single carboxyl placed in a molecularly imprinted active site is able to hydrolyze aryl glucosides with about 1/135 of the efficiency of some natural enzymes. One benefit of a cross-linked polymeric nanoparticle catalyst is its stability under harsh reaction conditions and recyclability as a result.[23] This work demonstrates that aromatic interactions can be employed strategically to help distinguish aromatic guests with similar size, shape, charge character but different π electron density. More importantly, a similar strategy enables our synthetic catalysts to override the intrinsic reactivity of aryl glycosides, so that the substrate that is almost 10 times less reactive becomes 3 times more reactive, to mimic nucleoside hydrolase of the parasite Trypanosoma vivax.[28]

## ASSOCIATED CONTENT

### Data Availability Statement

The data underlying this study are available in the published article and its Supporting Information.

### Supporting Information

Synthetic procedures, characterization data, ITC titration curves, additional data, and NMR spectra. This material is available free of charge via the Internet at http://pubs.acs.org.

## AUTHOR INFORMATION

### Corresponding Author

Yan Zhao – Department of Chemistry, Iowa State University, Ames, Iowa 50011-3111, U.S.A.; E-mail: zhaoy@iastate.edu*

### Author

Foroogh Bahrami - Department of Chemistry, Iowa State University, Ames, Iowa 50011-3111, U.S.A.

### Notes

The authors declare no competing financial interests.

## ACKNOWLEDGMENT

We thank NSF (CHE-2246635) for supporting the research. We thank Dr. Avijit Ghosh at Iowa State University for providing a sample of **1c**.

## REFERENCES

(1) Hunter, C. A.; Lawson, K. R.; Perkins, J.; Urch, C. J. Aromatic interactions. *J. Chem. Soc. Perkin Trans. 2* **2001**, 651-669.
(2) Mahadevi, A. S.; Sastry, G. N. Cation– π interaction: Its role and relevance in chemistry, biology, and material science. *Chem. Rev.* **2013**, *113*, 2100-2138.
(3) Zhao, Y.; Cotelle, Y.; Liu, L.; López-Andarias, J.; Bornhof, A.-B.; Akamatsu, M.; Sakai, N.; Matile, S. The emergence of anion–π catalysis. *Acc. Chem. Res.* **2018**, *51*, 2255-2263.
(4) Neel, A. J.; Hilton, M. J.; Sigman, M. S.; Toste, F. D. Exploiting non-covalent π interactions for catalyst design. *Nature* **2017**, *543*, 637-646.
(5) Wang, D.-X.; Wang, M.-X. Exploring Anion– π Interactions and Their Applications in Supramolecular Chemistry. *Acc. Chem. Res.* **2020**, *53*, 1364-1380.
(6) Sun, M.; Lee, M. Switchable aromatic nanopore structures: functions and applications. *Acc. Chem. Res.* **2021**, *54*, 2959-2968.
(7) Nerinckx, W.; Desmet, T.; Claeyssens, M. A hydrophobic platform as a mechanistically relevant transition state stabilising factor appears to be present in the active centre of all glycoside hydrolases. *FEBS Lett.* **2003**, *538*, 1-7.
(8) Montalvillo-Jiménez, L.; Santana, A. G.; Corzana, F.; Jiménez-Osés, G.; Jiménez-Barbero, J.; Gómez, A. M.; Asensio, J. L. Impact of Aromatic Stacking on Glycoside Reactivity: Balancing CH/π and Cation/π Interactions for the Stabilization of Glycosyl-Oxocarbenium Ions. *J. Am. Chem. Soc.* **2019**, *141*, 13372-13384.
(9) Zhou, Z.; Swenson, R. P. The Cumulative Electrostatic Effect of Aromatic Stacking Interactions and the Negative Electrostatic Environment of the Flavin Mononucleotide Binding Site Is a Major Determinant of the Reduction Potential for the Flavodoxin from Desulfovibrio vulgaris [Hildenborough]. *Biochemistry* **1996**, *35*, 15980-15988.
(10) Wulff, G.; Liu, J. Design of biomimetic catalysts by molecular imprinting in synthetic polymers: the role of transition state stabilization. *Acc. Chem. Res.* **2012**, *45*, 239-247.
(11) Shen, X.; Huang, C.; Shinde, S.; Jagadeesan, K. K.; Ekström, S.; Fritz, E.; Sellergren, B. Catalytic Formation of Disulfide Bonds in Peptides by Molecularly Imprinted Microgels at Oil/Water Interfaces. *ACS Appl. Mater. Interfaces* **2016**, *8*, 30484-30491.
(12) Yuan, Y.; Yang, Y.; Faheem, M.; Zou, X.; Ma, X.; Wang, Z.; Meng, Q.; Wang, L.; Zhao, S.; Zhu, G. Molecularly Imprinted Porous Aromatic Frameworks Serving as Porous Artificial Enzymes. *Adv. Mater.* **2018**, *30*, 1800069.
(13) Pan, J.; Chen, W.; Ma, Y.; Pan, G. Molecularly imprinted polymers as receptor mimics for selective cell recognition. *Chem. Soc. Rev.* **2018**, *47*, 5574-5587.
(14) Li, S.; Lieberzeit, P. A.; Piletsky, S.; Turner, A. P. F.: *Smart polymer catalysts and tunable catalysis*; Elsevier: Amsterdam, Netherlands ; Cambridge, MA, 2019.
(15) Zhang, H. Molecularly Imprinted Nanoparticles for Biomedical Applications. *Adv. Mater.* **2020**, *32*, 1806328.
(16) Haupt, K.; Medina Rangel, P. X.; Bui, B. T. S. Molecularly Imprinted Polymers: Antibody Mimics for Bioimaging and Therapy. *Chem. Rev.* **2020**, *120*, 9554-9582.
(17) Muratsugu, S.; Shirai, S.; Tada, M. Recent progress in molecularly imprinted approach for catalysis. *Tetrahedron Lett* **2020**, *61*, 151603.
(18) Li, J.; Zhu, M.; Wang, M.; Qi, W.; Su, R.; He, Z. Molecularly imprinted peptide-based enzyme mimics with enhanced activity and specificity. *Soft Matter* **2020**, *16*, 7033-7039.
(19) Wei, W.; Thakur, V. K.; Chew, Y. J.; Li, S. Towards next generation "smart" tandem catalysts with sandwiched mussel-inspired layer switch. *Mater. Today Chem.* **2020**, *17*, 100286.
(20) Chen, K.; Zhao, Y. Effects of nano-confinement and conformational mobility on molecular imprinting of cross-linked micelles. *Org. Biomol. Chem.* **2019**, *17*, 8611-8617.
(21) Arifuzzaman, M. D.; Bose, I.; Bahrami, F.; Zhao, Y. Imprinted polymeric nanoparticles as artificial enzymes for ester hydrolysis at room temperature and pH 7. *Chem Catal.* **2022**, *2*, 2049-2065.
(22) Bose, I.; Zhao, Y. Site-Selective Catalytic Epoxidation of Alkenes with Tunable Atomic Precision by Molecularly Imprinted Artificial Epoxidases. *ACS Catal.* **2022**, *12*, 3444-3451.
(23) Zangiabadi, M.; Zhao, Y. Synergistic Hydrolysis of Cellulose by a Blend of Cellulase-Mimicking Polymeric Nanoparticle Catalysts. *J. Am. Chem. Soc.* **2022**, *144*, 17110-17119.
(24) Ortega-Caballero, F.; Rousseau, C.; Christensen, B.; Petersen, T. E.; Bols, M. Remarkable supramolecular catalysis of glycoside hydrolysis by a cyclodextrin cyanohydrin. *J. Am. Chem. Soc.* **2005**, *127*, 3238-3239.
(25) Striegler, S.; Barnett, J. D.; Dunaway, N. A. Glycoside Hydrolysis with Sugar-Templated Microgel Catalysts. *ACS Catal.* **2012**, *2*, 50-55.
(26) Samanta, M.; Krishna, V. S. R.; Bandyopadhyay, S. A photoresponsive glycosidase mimic. *Chem. Commun.* **2014**, *50*, 10577-10579.
(27) Sharma, B.; Striegler, S. Nanogel Catalysts for the Hydrolysis of Underivatized Disaccharides Identified by a Fast Screening Assay. *ACS Catal.* **2023**, *13*, 1614-1620.
(28) Versées, W.; Loverix, S.; Vandemeulebroucke, A.; Geerlings, P.; Steyaert, J. Leaving group activation by aromatic stacking: an alternative to general acid catalysis. *J. Mol. Biol.* **2004**, *338*, 1-6.
(29) Zangiabadi, M.; Zhao, Y. Selective Binding of Complex Glycans and Glycoproteins in Water by Molecularly Imprinted Nanoparticles. *Nano Lett.* **2020**, *20*, 5106-5110.
(30) Zechel, D. L.; Withers, S. G. Glycosidase mechanisms: Anatomy of a finely tuned catalyst. *Acc. Chem. Res.* **2000**, *33*, 11-18.
(31) Dunn, B. M. Structure and Mechanism of the Pepsin-Like Family of Aspartic Peptidases. *Chem. Rev.* **2002**, *102*, 4431-4458.
(32) Westheimer, F. H. Coincidences, decarboxylation, and electrostatic effects. *Tetrahedron* **1995**, *51*, 3-20.
(33) Marquez, C.; Nau, W. M. Two Mechanisms of Slow Host–Guest Complexation between Cucurbit[6]uril and Cyclohexylmethylamine: pH-Responsive Supramolecular Kinetics. *Angew. Chem. Int. Ed.* **2001**, *40*, 3155-3160.
(34) Bakirci, H.; Koner, A. L.; Schwarzlose, T.; Nau, W. M. Analysis of Host-Assisted Guest Protonation Exemplified for p-Sulfonatocalix[4]arene—Towards Enzyme-Mimetic pKa Shifts. *Chem. -Eur. J.* **2006**, *12*, 4799-4807.
(35) Widanapathirana, L.; Zhao, Y. Tuning Nanopore Formation of Oligocholate Macrocycles by Carboxylic Acid Dimerization in Lipid Membranes. *J. Org. Chem.* **2013**, *78*, 4610-4614.
(36) Zmudka, M. W.; Thoden, J. B.; Holden, H. M. The structure of DesR from Streptomyces venezuelae, a β-glucosidase involved in macrolide activation. *Protein Sci.* **2013**, *22*, 883-892.
(37) Zhou, J.; Zhang, R.; Shi, P.; Huang, H.; Meng, K.; Yuan, T.; Yang, P.; Yao, B. A novel low-temperature-active β-glucosidase from symbiotic Serratia sp. TN49 reveals four essential positions for substrate accommodation. *Appl. Microbiol. Biotechnol.* **2011**, *92*, 305-315.
(38) Florindo, R. N.; Souza, V. P.; Manzine, L. R.; Camilo, C. M.; Marana, S. R.; Polikarpov, I.; Nascimento, A. S. Structural and biochemical characterization of a GH3 β-glucosidase from the probiotic bacteria Bifidobacterium adolescentis. *Biochimie* **2018**, *148*, 107-115.

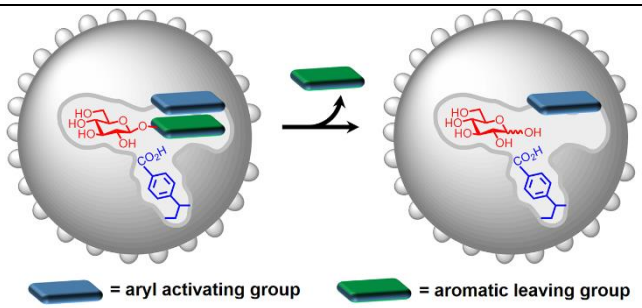
= aryl activating group
= aromatic leaving group